Turkish J. Eng. Env. Sci.
32 (2008) , 337 – 356.

Developing a Large Eddy Simulation Model (2DH FLOWER_SD) for Flow Modeling in Compound Channels

M. ADJAMI
Marine and Hydraulic Group, Civil Engineering Department, Faculty of Engineering, Tarbiat Modares University (TMU), Po. Box, 14115-143, Tehran-IRAN
e-mail: adjami@modares.ac.ir
M. SHAFIEEFAR
Marine and Hydraulic Group, Civil Engineering Department, Faculty of Engineering, Tarbiat Modares University (TMU), Po. Box, 14115-143, Tehran-IRAN
A. A. SALEHI NEYSHABORI
Marine and Hydraulic Group, Civil Engineering Department, Faculty of Engineering, Tarbiat Modares University (TMU), Po. Box, 14115-143, Tehran-IRAN

Received 05.09.2008

Abstract

As a compound channel is characterized by a deep main channel flanked by relatively shallow floodplains, the interaction between the faster fluid velocity in the main channel and the slower moving flow on the floodplains causes shear stress at their interface, which significantly distorts flow and boundary shear stress patterns. The distortion implies that the flow field in rivers is non-homogeneously turbulent, and that lateral transport of fluid momentum and suspended sediment are influenced by the characteristics of flow in rivers. The nature of the mechanism of lateral transport needs to be understood for the design of engineering schemes that rely upon realistic flow.

Furthermore, the flow in rivers is also almost turbulent. This means that the fluid motion is highly random, unsteady, and 3-dimensional. Thus, the flow cannot be properly predicted by using approximate analytical solutions to the governing equations of motion. With the complexity of the problem, the solution of turbulence is simplified with mathematical equations.

The newly developed Large Eddy Simulation 2DH FLOWER_SD[1] model was used to solve the turbulence problem. The successive over-relaxation method was employed to solve the numerical computation based on finite difference discretization. The model was applied to compound channels with smooth roughness. Some organized large eddies were observed in the boundary between the main channel and flood channel. At this boundary the transverse velocity profile exhibited a steep gradient, which induced significant mass and momentum exchange, acted as a source of vorticity, and generated high Reynolds stresses.

Key Words: Large eddy simulation, Compound channel, Turbulent flow, Navier-Stokes equations.

Introduction

The flow in a channel or conduit with a free surface is known as free surface flow or open channel flow (Chaudry, 1993). Flows in rivers, streams, irrigation or power canals, flumes, chutes, aqueducts, spillways, and drainage ditches are typical examples of free surface flows. For many problems encountered by hydraulic engineers, the analysis of free surface flow is required, e.g. heat and mass transport, dis-

[1]The 2DH FLOWER_SD source code (a reduced version of FLOWER_AD 3D flow solver written by Adjami et al.). freely available upon request; please contact adjami@modares.ac.ir

persion and dilution of pollutants, flood forecasting, and erosion and siltation in rivers and man-made canals.

A compound channel is a naturally occurring feature of any river or stream. Many rivers consist of a channel with adjacent floodplains. The bottom of the floodplain is generally rougher than and not as deep as the bottom of the main channel, so that during flooding the river consists of a relatively deep channel and shallow floodplains, a so-called compound channel. The word compound refers to the channel's ability to handle 2 stages of flow: normal flow and flood flow. Some of the main hydraulic features of compound channel flow for a symmetric 2-stage channel with a trapezoidal cross-section are shown in Figure 1.

As a compound channel is characterized by a deep main channel flanked by relatively shallow flood plains, the interaction between the higher fluid velocities in the main channel and the slower moving flow on the floodplains causes shear stresses at their interface, which significantly distort flow and boundary shear stress patterns. This distortion implies that the flow field in rivers is highly non-homogeneously turbulent, in which lateral transport of fluid momentum and suspended sediment are influenced by the characteristics of river flow. The mechanism of lateral transport needs to be understood in order to design river engineering schemes that rely upon realistic flow or sediment routing models.

Furthermore, river flow is mainly categorized as shallow water flow in which the horizontal scale of flow geometry is much larger than the vertical scale. Additionally, river flow is also almost turbulent, which means that the fluid motion is very random, unsteady, and 3-dimensional. Due to these complexities flow cannot be accurately predicted using approximate analytical solutions to the governing equations of motion. With the complexity of the problem, the solution of turbulence is simplified with mathematical equations.

Despite recent advances in computer technology, the storage capacity and speed of present day computers is not sufficient to compute turbulence, or, in other words, perhaps it will never be possible to mathematically simulate true turbulence with a computer. In order to circumvent this situation, turbulence fluctuations are approximated with a suitable averaging of the governing equations. These averaged equations describe the complete effect of turbulence on average motion. This representation is usually referred to as turbulence modeling.

During the last 2 decades many turbulence models were developed. There are 3 main turbulence models for a turbulent flow based on Navier Stokes equations: the Reynolds Averaged Navier Stokes simulation (RANS), Direct Numerical Simulation (DNS), and Large Eddy Simulation (LES). Based on the LES method, the 2DH module of the FLOWER_SD model is employed to study horizontal vortices.

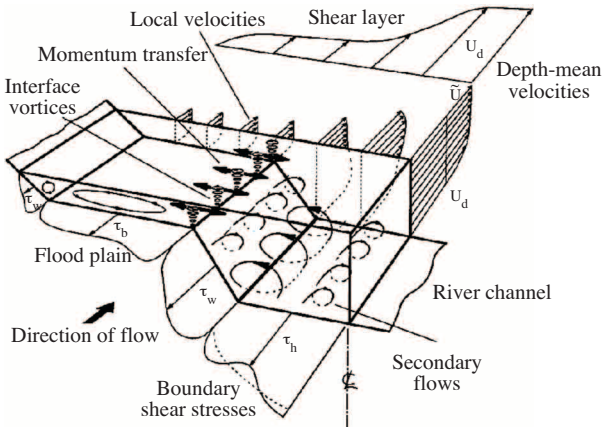

Figure 1. Hydraulic parameters associated with floodplain flow in a compound channel (Shiono and Knight, 2000).

The "2DH FLOWER_SD" Equations

As the phenomenon to be investigated was mainly 2-dimensional, a depth-averaged model was preferred to a complete 3-dimensional model solving the Navier-Stokes equations, so as to limit the computational cost.

The turbulence structure of a shallow water flow is characterized by the coexistence of 3D turbulence, having length scales less than the water depth, and horizontal 2-dimensional eddies with much larger length scales. As a result, the spectral structure of such a flow can be depicted as in Figure 2; the first peak corresponds to the horizontal 2D vortices generated by the transverse shearing. In this area, an inverse cascade of spectral energy can be observed as a result of processes like vortex pairing, while a direct attenuation also exists due to dissipation due to bottom friction.

A part of this dissipated energy may be supplied to the 3D turbulence at a higher wave-number (αp, while bottom friction may also directly provide 3D turbulent energy.

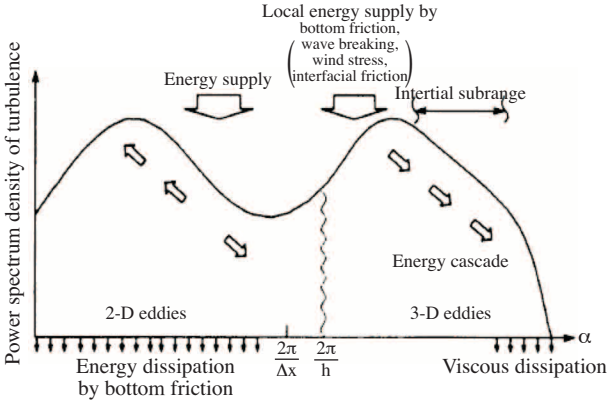

Figure 2. Turbulent energy spectrum in a depth-averaged flow with a shear layer (Nadaoka and Yagi, 1998).

The proposed FLOWER_SD model is similar in principle to LES, according to the length scales to be modeled. Indeed, similarly to the FLOWER_SD model, LES models explicitly solve the large turbulence scales, while the smaller scales are modeled implicitly, using a so-called subgrid model; however, when the grid size is reduced LES results tend to be similar to the results obtained from DNS simulation, in which all turbulence scales that correspond to molecular dissipation are modeled. This means that when decreasing the grid size an LES subgrid model will converge towards molecular viscosity.

Based on LES modeling concepts previously described (Deardof, 1970 [with some consideration due to Salvetti, 1995 for the sgs model]); Nadaoka, 1998; McDonough, 2004), the FLOWER_SD equations are derived:

$$\frac{\partial \overline{u}}{\partial x} + \frac{\partial \overline{v}}{\partial y} + \frac{\partial \overline{w}}{\partial z} = 0 \tag{1}$$

$$\frac{\partial \overline{u}}{\partial t} + \overline{u}\frac{\partial \overline{u}}{\partial x} + \overline{v}\frac{\partial \overline{u}}{\partial y} + \overline{w}\frac{\partial \overline{u}}{\partial z} = -\frac{1}{\rho_0}\frac{\partial \overline{p}}{\partial x}$$
$$+\upsilon\left(\frac{\partial^2 \overline{u}}{\partial x^2} + \frac{\partial^2 \overline{u}}{\partial y^2} + \frac{\partial^2 \overline{u}}{\partial z^2}\right) - \left(\frac{\partial \overline{u'u'}}{\partial x} + \frac{\partial \overline{u'v'}}{\partial y} + \frac{\partial \overline{u'w'}}{\partial z}\right) \tag{2}$$

$$\frac{\partial \overline{v}}{\partial t} + \overline{u}\frac{\partial \overline{v}}{\partial x} + \overline{v}\frac{\partial \overline{v}}{\partial y} + \overline{w}\frac{\partial \overline{v}}{\partial z} = -\frac{1}{\rho_0}\frac{\partial \overline{p}}{\partial y}$$
$$+\upsilon\left(\frac{\partial^2 \overline{v}}{\partial x^2} + \frac{\partial^2 \overline{v}}{\partial y^2} + \frac{\partial^2 \overline{v}}{\partial z^2}\right) - \left(\frac{\partial \overline{v'u'}}{\partial x} + \frac{\partial \overline{v'v'}}{\partial y} + \frac{\partial \overline{v'w'}}{\partial z}\right) \tag{3}$$

Flow domain

The general flow field sketch is presented in Figure 3. Where x, y, and $z$are, respectively, the longitudinal, transverse, and vertical directions, u, v, and $w$are the local velocity components in the x-, y-, and z-directions, respectively, p is the pressure, ρ is the density of water, $g$is the gravity constant, and υ is the molecular viscosity.

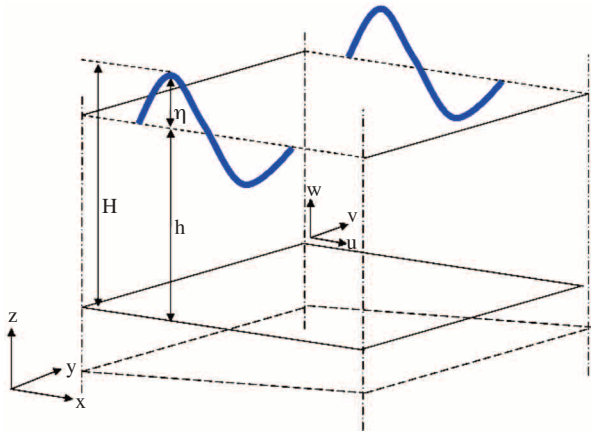

Figure 3. Definition sketch of the axial directions and velocity components (from VAMIT software manual).

Spatial filtering (LES method) was used, where$\overline{u}$,$\overline{v}$,$\overline{w}$, and $\overline{p}$ are the resolved components and u',v',w', and p' are the residual (subgrid) components. These forms are similar to that of Reynolds-averaging, where $\overline{u}$,$\overline{v}$ and $\overline{w}$ are the Reynolds-averaged velocities, and u', v', and $w'$are their turbulent fluctuations, whose products define Reynolds turbulent stresses. In the present study the shear stresses due to molecular viscosity will be negligible compared to the Reynolds stresses, as they are usually several orders of magnitude smaller.

Depth-integration will be performed along the z-direction, between the bed level (–h) and the free-surface water level (η). The depth-integrated longitudinal $U$and transverse Vvelocity components are thus defined as

$$U = \frac{1}{h+\eta}\int_{-h}^{\eta} \overline{u}dz \quad V = \frac{1}{h+\eta}\int_{-h}^{\eta} \overline{v}dz \tag{4}$$

The total water column height is defined as:

$$H = h + \eta \tag{5}$$

Free surface boundary

The free-surface boundary condition is defined by assuming that a particle present on the surface at a given time will remain there. The free-surface is thus defined by

$$S(x,y,z,t) = \eta(x,y,t) - z = 0 \tag{6}$$

simply expressing that the variable $z$gets the value η and defines the free-surface. The substantial derivative D/Dt of this equation equals zero, which means that a particle on the free-surface remains on the surface, thus giving

$$\begin{aligned}
&\frac{dS}{dt} = 0 :, \frac{dS}{dt} = \frac{\partial \eta}{\partial t} + \frac{\partial \eta}{\partial x}\frac{\partial x}{\partial t} + \frac{\partial \eta}{\partial y}\frac{\partial y}{\partial t} - \frac{\partial z}{\partial t} = 0,\\
&\text{hence } \frac{\partial \eta}{\partial t} + u\frac{\partial \eta}{\partial x} + v\frac{\partial \eta}{\partial y} - w = 0\\
&\overline{w}|_{z=\eta} = \left.\frac{D\eta}{Dt}\right|_{z=\eta} = \frac{\partial \eta}{\partial t} + \overline{u}|_{z=\eta}\frac{\partial \eta}{\partial x} + \overline{v}|_{z=\eta}\frac{\partial \eta}{\partial y}\\
&-\left[\overline{u}\frac{\partial \eta}{\partial x} + \overline{v}\frac{\partial \eta}{\partial y} - \overline{w}\right]_{z=\eta} = \frac{\partial \eta}{\partial t}
\end{aligned} \tag{7}$$

Bottom surface boundary

The bottom boundary condition is obtained similarly:

$$S(x,y,z,t) = z_0(x,y,t) - z = 0, with \frac{dS}{dt} = 0 :$$

$$\frac{dS}{dt} = \frac{\partial z_0}{\partial t} + \frac{\partial z_0}{\partial x}\frac{\partial x}{\partial t} + \frac{\partial z_0}{\partial y}\frac{\partial y}{\partial t} + \frac{\partial z}{\partial t} = 0$$

$$\frac{\partial z_0}{\partial t} + u(x,y,z_0)\frac{\partial z_0}{\partial x} + v(x,y,z_0)\frac{\partial z_0}{\partial y} + w(x,y,z_0) = 0$$

at $z = z_0$

The velocity at the bottom is *U(-h) = V(-h) = W(-h) = 0*, then $\frac{\partial h}{\partial t} = 0$

$$\left[\overline{u}\frac{\partial(-h)}{\partial x} + \overline{v}\frac{\partial(-h)}{\partial y} - \overline{w}\right]_{z=-h} = 0 \tag{8}$$

Depth averaged continuity equations

Integrating the continuity equation (1) along the depth gives

$$\int_{-h}^{\eta}\left(\frac{\partial \overline{u}}{\partial x} + \frac{\partial \overline{v}}{\partial y} + \frac{\partial \overline{w}}{\partial z}\right)dz = 0$$

where the integration and differentiation operators have to be inverted using the Leibnitz rule:

$$\int_{A(x,y,t)}^{B(x,y,t)}\frac{\partial F}{\partial x}dz = \frac{\partial}{\partial x}\int_{a}^{b}Fdz + F|_{z=A}\frac{\partial A}{\partial x} - F|_{z=B}\frac{\partial B}{\partial x} \tag{9}$$

$$\begin{aligned}
&\int_{-h}^{\eta}\left(\frac{\partial \overline{u}}{\partial x} + \frac{\partial \overline{v}}{\partial y} + \frac{\partial \overline{w}}{\partial z}\right)dz = \int_{-h(x,y,t)}^{\eta(x,y,t)}\frac{\partial \overline{u}}{\partial x}dz\\
&+ \int_{-h(x,y,t)}^{\eta(x,y,t)}\frac{\partial \overline{v}}{\partial y}dz + \int_{-h}^{\eta}\left(\frac{\partial \overline{w}}{\partial z}\right)dz = 0\\
&\int_{-h(x,y,t)}^{\eta(x,y,t)}\frac{\partial \overline{u}}{\partial x}dz + \int_{-h(x,y,t)}^{\eta(x,y,t)}\frac{\partial \overline{v}}{\partial y}dz + \overline{w}(\eta) - \overline{w}(-h) = 0
\end{aligned} \tag{10}$$

The 3 terms on the left side of (10) are thus written as

$$\int_{-h}^{\eta}\frac{\partial \overline{u}}{\partial x}dz = \frac{\partial}{\partial x}\int_{-h}^{\eta}\overline{u}dz + \overline{u}|_{z=-h}\frac{\partial h}{\partial x} - \overline{u}|_{z=\eta}\frac{\partial \eta}{\partial x}$$

$$\int_{-h}^{\eta}\frac{\partial \overline{v}}{\partial y}dz = \frac{\partial}{\partial y}\int_{-h}^{\eta}\overline{v}dz + \overline{v}|_{z=-h}\frac{\partial(-h)}{\partial y} - \overline{v}|_{z=\eta}\frac{\partial \eta}{\partial y}$$

$$\int_{-h}^{\eta}\frac{\partial \overline{w}}{\partial z}dz = \overline{w}|_{z=\eta} - \overline{w}|_{z=-h}$$

Grouping again those 3 terms and using the definitions of depth-integrated velocities

$$\begin{aligned}
&\frac{\partial}{\partial x}\int_{-h}^{\eta}\overline{u}dz + \frac{\partial}{\partial y}\int_{-h}^{\eta}\overline{v}dz - \left[\overline{u}\frac{\partial \eta}{\partial x} + \overline{v}\frac{\partial \eta}{\partial y} - \overline{w}\right]_{z=\eta}\\
&+\left[\overline{u}\frac{\partial(-h)}{\partial x} + \overline{v}\frac{\partial(-h)}{\partial y} - \overline{w}\right]_{z=(-h)} = 0
\end{aligned} \tag{11}$$

U and V given by (4), and boundary conditions given by (7) and (8) the continuity equation becomes

$$\frac{\partial \eta}{\partial t} + \frac{\partial}{\partial x}\int_{-h}^{\eta}\overline{u}dz + \frac{\partial}{\partial y}\int_{-h}^{\eta}\overline{v}dz = 0 \tag{12}$$

$$\frac{\partial \eta}{\partial t} + \frac{\partial[(\eta+h)U]}{\partial x} + \frac{d[(\eta+h)V]}{dy} = 0 \tag{13}$$

Depth integrated momentum equations

When the momentum equation in the x direction (2) is integrated along the depth (z), one obtains

$$\underbrace{\int_{-h}^{\eta}\frac{d\overline{u}}{dt}dz}_{\text{term1}}+\underbrace{\int_{-h}^{\eta}\frac{\partial\overline{uu}}{\partial x}dz}_{\text{term2}}+\underbrace{\int_{-h}^{\eta}\frac{\partial\overline{uv}}{\partial y}dz}_{\text{term3}}+\underbrace{\int_{-h}^{\eta}\frac{\partial\overline{uw}}{\partial z}dz}_{\text{term4}}=\underbrace{-\frac{1}{\rho}\int_{-h}^{\eta}\frac{\partial\overline{p}}{\partial x}dz}_{\text{term5}}+\underbrace{\int_{-h}^{\eta}\left(\frac{\partial}{\partial x}\overline{u'u'}+\frac{\partial}{\partial y}\overline{u'v'}+\frac{\partial}{\partial z}\overline{v'w'}\right)dz}_{\text{term6}} \tag{14}$$

Term 1

As for the continuity equation, the Leibnitz rule is used to invert the integration and derivation operators. Using the fixed bed hypothesis and the definition of depth-averaged longitudinal velocity U (4), the acceleration term, the first term on the left side of (14), gives

$$\int_{-h}^{\eta}\frac{\partial\overline{u}}{\partial t}dz=\frac{\partial}{\partial t}\int_{-h}^{\eta}\overline{u}dz-\overline{u}|_{z=\eta}\frac{\partial(\eta)}{\partial t}+\overline{u}|_{z=-h}\frac{\partial(-h)}{\partial t}=\frac{\partial}{\partial t}(UH)-\overline{u}|_{z=\eta}\frac{\partial(\eta)}{\partial t} \tag{15}$$

Term 2

The first convection term, the second term on the left side of (14), gives

$$\int_{-h}^{\eta}\frac{\partial\overline{uu}}{\partial x}dz=\frac{\partial}{\partial x}\int_{-h}^{\eta}\overline{u}^2dz-\overline{u}^2\big|_{z=\eta}\frac{\partial(\eta)}{\partial x}+\overline{u}^2\big|_{z=-h}\frac{\partial(-h)}{\partial x} \tag{16}$$

The integration of the velocity product ($\overline{u}^2$) in the first term on the right side of (16) will generate the first dispersion term. Indeed, one expects to express this term as a function of the depth-averaged longitudinal velocity (U). The depth-integration of its squared value is thus different from the square of the depth-averaged velocity (U). Several authors suggest using the so-called Boussinesq coefficient (β in order to take into account this difference (Liggett, 1994):

$$\beta_{xx}=\frac{1}{(\eta+h)U^2}\int_{-h}^{\eta}\overline{u}^2dz$$

However, most of these authors then assume that this Boussinesq coefficient equals βg 1, neglecting the dispersion effect.

The integration of the square of $\overline{u}$ in Eq. (16) can be written as

$$\int_{-h}^{\eta}\frac{\partial\overline{uu}}{\partial x}dz=\frac{\partial}{\partial x}\int_{-h}^{\eta}\overline{u}^2dz+\underbrace{\overline{u}^2(-h)\frac{\partial(-h)}{\partial x}}_{=0}-\overline{u}^2(\eta)\frac{\partial(\eta)}{\partial x} \tag{17}$$

where the second term on the right side equals zero, as the integration of $\overline{u}$along the depth equals U, and the third term is the so-called dispersion term. Finally, Eq. (17) gives

$$\int_{-h}^{\eta}\frac{\partial\overline{uu}}{\partial x}dz=\frac{\partial}{\partial x}\int_{-h}^{\eta}\overline{u}^2dz-\overline{u}^2(\eta)\frac{\partial(\eta)}{\partial x}=\frac{\partial}{\partial x}\left[\beta_{xx}(\eta+h)U^2\right]-\overline{u}^2(\eta)\frac{\partial(\eta)}{\partial x} \tag{18}$$

Term 3

In the same way, the second convection term in Eq. (14), Term 3, becomes

$$\int_{-h}^{\eta}\frac{\partial\overline{uv}}{\partial y}dz=\frac{\partial}{\partial y}\int_{-h}^{\eta}\overline{uv}dz+\underbrace{\overline{uv}(-h)\frac{\partial(-h)}{\partial y}}_{=0}-\overline{uv}(\eta)\frac{\partial(\eta)}{dy}=\frac{\partial}{\partial y}\int_{-h}^{\eta}\overline{uv}dz-\overline{uv}(\eta)\frac{\partial(\eta)}{\partial y}$$
$$\text{instance }\beta_{yx}=\frac{1}{(\eta+h)UV}\int_{-h}^{\eta}\overline{uv}dz$$
$$=\frac{\partial}{\partial y}\left[\beta_{yx}(\eta+h)UV\right]-\overline{uv}(\eta)\frac{\partial(\eta)}{\partial y} \tag{19}$$

Term 4

The third convection term of Eq. (14), Term 4 simplifies to

$$\int_{-h}^{\eta}\frac{\partial\overline{uw}}{\partial z}dz=\overline{uw}|_{-h}^{\eta}=\overline{w}|_{z=\eta}-\overline{w}|_{z=-h} \tag{20}$$

Term 5

When the Leibnitz rule is applied to the pressure term in Eq. (14), Term 5, the first term on the right side gives

$$\overline{p}=\rho g(\eta-z)+p_a$$

where the pressure (pa) at the free-surface is set to equal zero:

$$\begin{aligned}
\frac{1}{\rho}\int_{-h}^{\eta}\frac{\partial\overline{p}}{\partial x}dz &= \frac{1}{\rho}\frac{\partial}{\partial x}\int_{-h}^{\eta}\overline{p}dz - \frac{\overline{p}}{\rho}\Big|_{z=\eta}\frac{\partial\eta}{\partial x} + \frac{\overline{p}}{\rho}\Big|_{z=-h}\frac{\partial(-h)}{\partial x} \\
\frac{1}{\rho}\int_{-h}^{\eta}\frac{\partial\overline{p}}{\partial x}dz &= \frac{1}{\rho}\frac{\partial}{\partial x}\int_{-h}^{\eta}\rho g\left(\eta-z\right)dz - \frac{\rho g\left(\eta-\eta\right)}{\rho}\frac{\partial\eta}{\partial x} + \frac{\rho g\left(\eta-(-h)\right)}{\rho}\frac{\partial(-h)}{\partial x} \\
&= g\frac{\partial}{\partial x}\left(\eta\left(\eta-(-h)\right)-\frac{1}{2}\left(\eta^2-(-h)^2\right)\right)+gH\frac{\partial(-h)}{\partial x} = g\frac{\partial}{\partial x}\frac{1}{2}H^2+gH\frac{\partial(-h)}{\partial x} \qquad (21)\\
\text{where } S_0 &= \frac{\partial(-h)}{\partial x} \qquad (22)
\end{aligned}$$

Term 6

Lastly, again using the Leibnitz rule, the shear-stress terms become

$$\begin{aligned}
\int_{-h}^{\eta}\left(\frac{\partial z}{\partial x}\overline{u'u'}+\frac{\partial}{\partial y}\overline{u'v'}+\frac{\partial}{\partial z}\overline{u'w'}\right)dz &= \frac{\partial}{\partial x}\int_{-h}^{\eta}\overline{u'u'}dz - \left(\overline{u'u'}\right)\big|_{z=\eta}\frac{\partial\eta}{\partial x} + \left(\overline{u'u'}\right)\big|_{z=-h}\frac{\partial\left(-h\right)}{\partial x} \\
&+\frac{\partial}{\partial y}\int_{-h}^{\eta}\overline{u'v'}dz - \left(\overline{u'v'}\right)\big|_{z=\eta}\frac{\partial\eta}{\partial y} + \left(\overline{u'v'}\right)\big|_{z=-h}\frac{\partial\left(-h\right)}{\partial y} \qquad (23)\\
&+\left(\overline{u'w'}\right)\big|_{z=\eta} - \left(\overline{u'w'}\right)\big|_{z=-h}
\end{aligned}$$

It is then assumed that the shear stress at the free-surface is negligible. The 2nd, 5th, and 7th terms on the right side of Eq. (23) thus equal zero. On the other hand, regarding the shear stresses at the bed, the 3rd and 6th terms (stresses along vertical planes) will be assumed to be negligible compared to the 18th term (stress along the horizontal plane). The shear stress terms (23) thus reduce to

$$\int_{-h}^{\eta}\left(\frac{\partial z}{\partial x}\overline{u'u'}+\frac{\partial}{\partial y}\overline{u'v'}+\frac{\partial}{\partial z}\overline{u'w'}\right)dz = \frac{\partial}{\partial x}\int_{-h}^{\eta}\overline{u'u'}dz+\frac{\partial}{\partial y}\int_{-h}^{\eta}\overline{u'v'}dz - \left(\overline{u'w'}\right)\big|_{z=-h} = \frac{\partial}{\partial x}\int_{-h}^{\eta}\overline{u'u'}dz+\frac{\partial}{\partial y}\int_{-h}^{\eta}\overline{u'v'}dz+\tau_{bx} \qquad (24)$$

The depth-averaged x-wise momentum Eq. (14) is obtained by the addition of Eqs. (15), (18), (19), (20), (21), and (24):

$$\begin{aligned}
&\frac{\partial}{\partial t}\left(UH\right)+\frac{\partial}{\partial x}\left(U^2H\right)+\frac{\partial}{\partial y}\left(UVH\right)dz-\overline{u}\left[\frac{\partial\eta}{\partial t}+\overline{u}\frac{\partial\eta}{\partial x}+\overline{v}\frac{\partial\eta}{\partial y}-\overline{w}\right]_{z=\eta}+\left[\overline{u}\frac{\partial\left(-h\right)}{\partial x}+\overline{v}\frac{\partial\left(-h\right)}{\partial y}-\overline{w}\right]_{z=-h} \\
&= -g\frac{\partial}{\partial x}{}^1\!/_2H^2-gH\frac{\partial(-h)}{\partial x}-\frac{\partial}{\partial x}\int_{-h}^{\eta}\overline{u'u'}dz-\frac{\partial}{\partial y}\int_{-h}^{\eta}\overline{u'v'}dz-\tau_{bx} \qquad (25)
\end{aligned}$$

where the last 2 terms on the left side equal zero due to the boundary conditions at the free surface (7) and the bed (8). Using the definitions (22) of the bed slope (S_0) and grouping the x-derivatives, one obtains

$$\frac{\partial}{\partial t}\left(UH\right)+\frac{\partial}{\partial x}\left(U^2H+{}^1\!/_2gH^2\right)+\frac{\partial}{\partial y}\left(UVH\right)=gHS_0-\tau_{bx}-\frac{\partial}{\partial x}\int_{-h}^{\eta}\overline{u'u'}dz-\frac{\partial}{\partial y}\int_{-h}^{\eta}\overline{u'v'}dz \qquad (26)$$

The so-called "non-conservative" form of Eq. (26) is obtained by subtracting the continuity equation (1) multiplied by U and dividing the resulting equation by H:

$$\frac{\partial U}{\partial t}+U\frac{\partial U}{\partial x}+V\frac{\partial U}{\partial y}=g\left(S_{0x}-S_{fx}\right)-g\frac{\partial H}{\partial x}-\frac{1}{H}\frac{\partial}{\partial x}\int_{-h}^{\eta}\overline{u'u'}dz-\frac{1}{H}\frac{\partial}{\partial y}\int_{-h}^{\eta}\overline{u'v'}dz-\tau_{bx} \tag{27}$$

$$\frac{\partial U}{\partial t}+U\frac{\partial U}{\partial x}+V\frac{\partial U}{\partial y}=gS_0-g\frac{\partial \eta}{\partial x}-\frac{1}{H}\frac{\partial}{\partial x}\int_{-h}^{\eta}\overline{u'u'}dz-\frac{1}{H}\frac{\partial}{\partial y}\int_{-h}^{\eta}\overline{u'v'}dz-\tau_{bx} \tag{28}$$

Reynolds stresses are defined as

$$-\frac{1}{H}\int_{-h}^{\eta}\overline{u_i'u_j'}dz-=\upsilon_t\left(\frac{\partial\overline{u_i}}{\partial x_j}+\frac{\partial\overline{u_j}}{\partial x_i}\right)-\frac{2}{3}\delta_{ij}k \tag{29}$$

where υt is the eddy viscosity, δij is the Kronecker symbol ($\delta ij = 1$ for $i = j$; and $\delta ij = 0$ for $i \neq j$), and k is the kinetic turbulent energy

$$\tau_{xx}=\left(2\upsilon_t\frac{\partial u}{\partial x}-\frac{2}{3}k\right),\quad \tau_{yy}=\left(2\upsilon_t\frac{\partial v}{\partial y}-\frac{2}{3}k\right) \tag{30}$$

$$\tau_{xy}=\tau_{yx}=\upsilon_t\left(\frac{\partial u}{\partial y}+\frac{\partial v}{\partial x}\right) \tag{31}$$

$$\tau_{bx}=\left(\frac{ac_d}{2}+\frac{c_f}{\eta+h}\right)u\sqrt{u^2+v^2} \tag{32}$$

where $\tau_{bx}$is defined as bottom stresses due to bottom friction and vegetation drag.

Writing back Eq. (28), one at last gets

$$\frac{\partial u}{\partial t}+u\frac{\partial u}{\partial x}+v\frac{\partial u}{\partial y}=-g\frac{\partial \eta}{\partial x}+gS_0-\left(\frac{ac_d}{2}+\frac{c_f}{\eta+h}\right)u\sqrt{u^2+v^2}+\frac{\partial}{\partial x}\left(2\upsilon_t\frac{\partial u}{\partial x}-\frac{2}{3}k\right)+\frac{\partial}{\partial y}\left[\upsilon_t\left(\frac{\partial v}{\partial x}+\frac{\partial u}{\partial y}\right)\right] \tag{33}$$

$$\frac{\partial v}{\partial t}+u\frac{\partial v}{\partial x}+v\frac{\partial v}{\partial y}=-g\frac{\partial \eta}{\partial y}-(\frac{ac_b}{2}+\frac{c_f}{\eta+h})v\sqrt{u^2+v^2}+\frac{\partial}{\partial y}\left(2\upsilon_t\frac{\partial v}{\partial y}-\frac{2}{3}k\right)+\frac{\partial}{\partial x}\left[\upsilon_t\left(\frac{\partial v}{\partial x}+\frac{\partial u}{\partial y}\right)\right] \tag{34}$$

Turbulence kinetic energy

The depth-averaged kinetic energy of turbulence (k) is evaluated with the following improved energy-transport equations:

$$\frac{Dk}{Dt}=\frac{\partial}{\partial x}\left(\frac{\upsilon_t}{\sigma_k}\frac{\partial k}{\partial x}\right)+\frac{\partial}{\partial y}\left(\frac{\upsilon_t}{\sigma_k}\frac{\partial k}{\partial y}\right)+P_{kh}+P_{kv}-\varepsilon \tag{35}$$

The eddy viscosity (υ_t) and the energy dissipation rate (ε) are evaluated by k and l according to the usual k-equation model:

$$\upsilon_t=C_\mu\frac{k^2}{\varepsilon} \tag{36}$$

$$\varepsilon=C_d\frac{k^{3/2}}{l} \tag{37}$$

For the model, parametersC_μ, C_d, and σ_k, the standard values $C_\mu = 0.09$, $C_d = 0.17$, and $\sigma_k = 1.0$ are adopted here.

The turbulence length-scale (l) is expressed as$l = \alpha h$, in which $\alpha = 0.1$ P_{kh} and P_{kv} are calculated with the following relations from Rastogi and Rodi (1978), with an additional term in P_{kv} due to vegetation drag (Rodi, 1980):

$$P_{kh}=\upsilon_t\left[2\left(\frac{\partial u}{\partial x}\right)^2+2\left(\frac{\partial v}{\partial y}\right)^2+2\left(\frac{\partial u}{\partial y}+\frac{\partial v}{\partial x}\right)^2\right] \tag{38}$$

$$P_{kv}=\left[\left(c_f+\frac{ac_dh}{2}\right)\left(u^2+v^2\right)\right]^{1.5}\Big/ l \tag{39}$$

The P_{kh} term corresponds to the turbulent kinetic energy production due to the interaction between the turbulent shear stress and the depth-averaged velocity gradient. The term P_{kv} is a source

term, which absorbs all the secondary terms originating from the non-uniformity of vertical profiles. The main contribution to this term arises from significant vertical velocity gradients near the bed. It expresses, therefore, the turbulent kinetic energy production due to bed friction and vegetation drag.

Numerical Solution

The 2DH FLOWER_SD equations are solved with the finite difference method, with which successive over relaxation (SOR) is applied to numerical computation. There exist a number of approaches for the discretization of those equations. A stable finite difference method is based on using a so-called staggered grid (McKibben, 1993) when the unknown variables, u, v, and η, lie at different grids shifted with respect to each other. Figure 4 shows the staggered grid scheme. That simple model of a staggered grid makes it possible to use simple discretization and prevent numerical instabilities from forming within the model.

The first spatial discretization makes use of a staggered "marker-and-cell" (MAC) mesh (Bousmar, 2002), slightly modified for shallow-water flow modeling. In such a mesh, the velocities (u and v) are defined for positions situated at a distance midway between the points where the water level (η) are defined (Figure 5). This location enables easy estimation of the water level (η) value at any point of interest (η, U, V) using a linear interpolation. Such a staggered mesh provides good coupling between the velocities and water depth, ensuring very good mass and momentum conservation during the resolution; this condition is indeed required for uniform-flow modeling with a cyclic boundary condition.

Additionally, the values of the viscosity (υt) and of the turbulent kinetic energy (k) are defined at the same locations as the water level (η). Each equation from (13), (23), (24), and (38) is then discretized with a computational molecule centered on the location at which the value varying with time is defined: at the water-level (η) definition point for the continuity equation (13) and for the turbulent kinetic energy transport equation (38); at the longitudinal-velocity (U) definition point for the x momentum equation (23); and at the transverse-velocity (V) definition point for the y momentum equation (24).

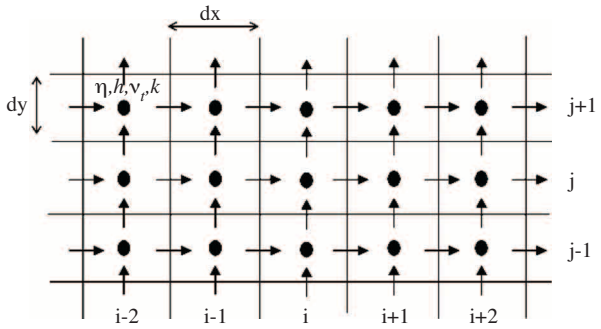

Figure 4. Staggered Grid MAC (Marker And Cell).

Continuity equation discretization

The continuity equation discretized on the staggered grid can be written as follows:

$$\begin{gathered}\frac{\partial \eta}{\partial t}+\frac{\partial}{\partial x}\left[(\eta+h)\,u\right]+\frac{d}{dy}\left[(\eta+h)\,v\right]=0\\ \frac{\left[\eta_{i,j}^{n+1}-\eta_{i,j}^{n}\right]}{\Delta t}+\frac{\left[\left(\eta_{i+1,j}^{n}+h_{i+1,j}^{n}\right)\left(\frac{u_{i+1,j}^{n}+u_{i+2,j}^{n}}{2}\right)-\left(p_{i-1,j}^{n}+\eta_{i-1,j}^{n}\right)\left(\frac{u_{i-1,j}^{n}+u_{i,j}^{n}}{2}\right)\right]}{2\Delta x}\\ +\frac{\left[\left(\eta_{i,j+1}^{n}+h_{i,j+1}^{n}\right)\left(\frac{v_{i,j+1}^{n}+v_{i,j+2}^{n}}{2}\right)-\left(\eta_{i,j-1}^{n}+h_{i,j-1}^{n}\right)\left(\frac{v_{i,j-1}^{n}+v_{i,j}^{n}}{2}\right)\right]}{2\Delta y}=0\end{gathered} \tag{40}$$

Momentum equation discretization

The momentum equations discretized on the staggered grid can be written as follows:

X-direction

$$\frac{\partial u}{\partial t}=-\left(u\frac{\partial u}{\partial x}+v\frac{\partial u}{\partial y}\right)-g\frac{\partial \eta}{\partial x}+gs_0-(\frac{ac_b}{2}+\frac{c_f}{\eta+h})u\sqrt{u^2+v^2}+\frac{\partial}{\partial x}\left(2\upsilon_t\frac{\partial u}{\partial x}-\frac{2}{3}k\right)+\frac{\partial}{\partial y}\left[\upsilon_t h\left(\frac{\partial v}{\partial x}+\frac{\partial u}{\partial y}\right)\right] \tag{41}$$

$$\frac{\partial u}{\partial t} = +A0^n_{i,j} - AP^n_{i,j} + AI^n_{i,j} + AF^n_{i,j} + AN^n_{i,j} \tag{42}$$

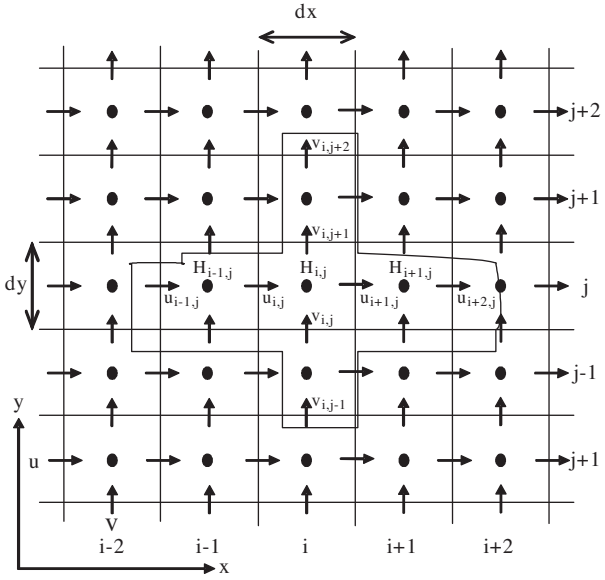

Figure 5. Points on a grid used for continuity equation solving.

Y-direction

$$\frac{\partial v}{\partial t} = -\left(u\frac{\partial v}{\partial x} + v\frac{\partial v}{\partial y}\right) - g\frac{\partial \eta}{\partial y} - (\frac{ac_b}{2} + \frac{c_f}{\eta + h})v\sqrt{u^2 + v^2} + \frac{\partial}{\partial y}\left(2\upsilon_t\frac{\partial v}{\partial y} - \frac{2}{3}k\right) + \frac{\partial}{\partial x}\left[\upsilon_t\left(\frac{\partial v}{\partial x} + \frac{\partial u}{\partial y}\right)\right] \tag{43}$$

$$\frac{\partial v}{\partial t} = +B0_{i,j,k} - BP_{i,j,k} + BI_{i,j,k} + BF_{i,j,k} + BN_{i,j,k} \tag{44}$$

Term in Left Hand Side (LHS)

$$\frac{\partial u}{\partial t} = \frac{u^{n+1}_{i,j} - u^n_{i,j}}{\Delta t} \tag{45}$$

$$\frac{\partial v}{\partial t} = \frac{v^{n+1}_{i,j} - v^n_{i,j}}{\Delta t} \tag{46}$$

Term on Left Hand Side (LHS)

$$-u\frac{\partial u}{\partial x} - v\frac{\partial u}{\partial y} = -\left(u\frac{\partial u}{\partial x} + v\frac{\partial u}{\partial y}\right) = A0^n_{i,j} \tag{47}$$

$$A0^n_{i,j} = -\left[\begin{array}{l} \dfrac{u^n_{i,j}}{\Delta x}\dfrac{\left[-u^n_{i+2,j} + 8\left(u^n_{i+1,j} - u^n_{i-1,j}\right) + u^n_{i-2,j}\right]}{12} \\ +\alpha\dfrac{ABS\left(u^n_{i,j}\right)}{\Delta x}\dfrac{\left[u^n_{i+2,j} - 4\left(u^n_{i+1,j} + u^n_{i-1,j}\right) + 6u^n_{i,j} + u^n_{i-2,j}\right]}{12} \\ +\dfrac{v^n_{i-1,j} + v^n_{i,j} + v^n_{i-1,j+1} + v^n_{i,j+1}}{4}\dfrac{1}{\Delta y}\dfrac{\left[-u^n_{i,j+2} + 8\left(u^n_{i,j+1} - u^n_{i,j-1}\right) + u^n_{i,j-2}\right]}{12} \\ +\alpha ABS\left(\dfrac{v^n_{i-1,j} + v^n_{i,j} + v^n_{i-1,j+1} + v^n_{i,j+1}}{4}\right)\dfrac{1}{\Delta y}\dfrac{\left[u^n_{i,j+2} - 4\left(u^n_{i,j+1} + u^n_{i,j-1}\right) + 6u^n_{i,j} + u^n_{i,j-2}\right]}{12} \end{array}\right] \tag{48}$$

Similar for y-direction:

$$-u\frac{\partial v}{\partial x}-v\frac{\partial v}{\partial y}=-\left(u\frac{\partial v}{\partial x}+v\frac{\partial v}{\partial y}\right)=B0_{i,j}^{n} \tag{49}$$

$$B0_{i,j}^{n}=-\left[\begin{array}{l}\frac{u_{i,j-1}^{n}+u_{i,j}^{n}+u_{i+1,j-1}^{n}+u_{i+1,j}^{n}}{4}\frac{1}{\Delta x}\frac{\left[-v_{i+2,j}^{n}+8\left(v_{i+1,j}^{n}-v_{i-1,j}^{n}\right)+v_{i-2,j}^{n}\right]}{12}\\ +\alpha ABS\left(\frac{u_{i,j-1}^{n}+u_{i,j}^{n}+u_{i+1,j-1}^{n}+u_{i+1,j}^{n}}{4}\right)\frac{1}{\Delta x}\frac{\left[v_{i+2,j}^{n}-4\left(v_{i+1,j}^{n}+v_{i-1,j}^{n}\right)+6v_{i,j}^{n}+v_{i-2,j}^{n}\right]}{4}\\ +\frac{v_{i,j}^{n}}{\Delta y}\frac{\left[-v_{i,j+2}^{n}+8\left(v_{i,j+1}^{n}-v_{i,j-1}^{n}\right)+v_{i,j-2}^{n}\right]}{12}\\ +\alpha\frac{ABS\left(v_{i,j}^{n}\right)}{\Delta y}\frac{\left[v_{i,j+2}^{n}-4\left(v_{i,j+1}^{n}-v_{i,j-1}^{n}\right)+6v_{i,j}^{n}+v_{i,j-2}^{n}\right]}{4}\end{array}\right] \tag{50}$$

In this computation $\alpha=3$ has been used. The scheme is known as the K-K (Kawamura-Kuwahara) scheme.

Second term on RHS

$$g\frac{\partial\eta}{\partial x}=AP_{i,j}^{n},\quad AP_{i,j}^{n}=g\frac{\left(\eta_{i+1,j}^{n}+2\eta_{i,j}^{n}-2\eta_{i-1,j}^{n}-\eta_{i-2,j}^{n}\right)}{2}\frac{1}{3}\frac{1}{\Delta x} \tag{51}$$

$$g\frac{\partial\eta}{\partial y}=BP_{i,j}^{n},\quad BP_{i,j}^{n}=g\frac{\left(\eta_{i,j+1}^{n}+2\eta_{i,j}^{n}-2\eta_{i,j-1}^{n}-\eta_{i,j-2}^{n}\right)}{2}\frac{1}{3}\frac{1}{\Delta y} \tag{52}$$

Third term on RHS

$$AI_{i,j}^{n}=gs_{0},\quad BI_{i,j}^{n}=0 \tag{53}$$

Fourth term on RHS

$$-\left(\frac{ac_{d}}{2}+\frac{c_{f}}{\eta+h}\right)u\sqrt{u^{2}+v^{2}}=AF_{i,j}^{n} \tag{54}$$

$$AF_{i,j}^{n}=-u_{i,j}^{n}\left(\frac{(ac_{d})_{i,j}^{n}}{2}+\frac{gn_{manning}^{2}\frac{\left(h_{i,j}^{n}{}^{-1/3}+h_{i-1,j}^{n}{}^{-1/3}\right)}{2}}{\left[\frac{\left(\eta_{i,j}^{n}+h_{i,j}^{n}\right)+\left(\eta_{i-1,j}^{n}+h_{i-1,j}^{n}\right)}{2}\right]}\right)\left(ABS\left(u_{i,j}^{n}\right)^{2}+ABS\left(\frac{v_{i-1,j}^{n}+v_{i,j}^{n}+v_{i-1,j+1}^{n}+v_{i,j+1}^{n}}{4}\right)^{2}\right) \tag{55}$$

$$-f_{y}-\frac{c_{f}}{\eta+h}v\sqrt{u^{2}+v^{2}}=BF_{i,j,k} \tag{56}$$

$$\begin{array}{l}BF_{i,j}^{n}=-v_{i,j}^{n}\left(\frac{(ac_{d})_{i,j}^{n}}{2}+\frac{gn_{manning}^{2}\frac{\left(h_{i,j}^{n}{}^{-1/3}+h_{i,j-1}^{n}{}^{-1/3}\right)}{2}}{\left[\frac{\left(\eta_{i,j}^{n}+h_{i,j}^{n}\right)+\left(\eta_{i,j-1}^{n}+h_{i,j-1}^{n}\right)}{2}\right]}\right)\\ \left(ABS\left(\frac{u_{i,j-1}^{n}+u_{i,j}^{n}+u_{i+1,j-1}^{n}+u_{i+1,j}^{n}}{4}\right)^{2}+ABS\left(v_{i,j}^{n}\right)^{2}\right)\end{array} \tag{57}$$

Fifth term on RHS

$$+\frac{\partial}{\partial x}\left(2\upsilon_{t}\frac{\partial u}{\partial x}-\frac{2}{3}k\right)+\frac{\partial}{\partial y}\left[\upsilon_{t}\left(\frac{\partial v}{\partial x}+\frac{\partial u}{\partial y}\right)\right]=AN_{i,j}^{n} \tag{58}$$

$$AN_{i,j}^{n}=\left[\left(\left(2,0\upsilon_{t_{i,j}}^{n}\frac{u_{i+1,j}^{n}}{\Delta x}\right)-\frac{2}{3}SDS_{i,j}^{n}\right)-\left(-\left(2,0\upsilon_{t_{i-1,j}}^{n}\frac{u_{i-1,j}^{n}}{\Delta x}\right)-\frac{2}{3}SDS_{i-1,j}^{n}\right)\right]\frac{1}{\Delta x}$$
$$+\left[\frac{\left(\upsilon_{t_{i,j+1}}^{n}+\upsilon_{t_{i-1,j+1}}^{n}\right)}{2}\left(\frac{\left(\upsilon_{i,j+1}^{n}+\upsilon_{i,j+2}^{n}\right)}{2}-\frac{\left(\upsilon_{i-1,j+1}^{n}+\upsilon_{i-1,j+2}^{n}\right)}{2}\right)\frac{1}{\Delta x}\right.$$
$$\left.-\frac{\left(\upsilon_{t_{i,j-1}}^{n}+\upsilon_{t_{i-1,j-1}}^{n}\right)}{2}\frac{\left(\upsilon_{i,j-1}^{n}+\upsilon_{i,j}^{n}\right)}{2}-\frac{\left(\upsilon_{i-1,j-1}^{n}+\upsilon_{i-1,j}^{n}\right)}{2}\frac{1}{\Delta x}\right]\frac{1}{2\Delta y} \tag{59}$$
$$+\frac{\left(\upsilon_{t_{i,j}}^{n}+\upsilon_{t_{i-1,j}}^{n}\right)}{2}\left(u_{i,j+1}^{n}+u_{i,j-1}^{n}\right)\frac{1}{\Delta y}\frac{1}{\Delta y}$$

$$+\frac{\partial}{\partial y}\left(2\upsilon_t\frac{\partial v}{\partial y}-\frac{2}{3}k\right)+\frac{\partial}{\partial x}\left[\upsilon_t\left(\frac{\partial v}{\partial x}+\frac{\partial u}{\partial y}\right)\right]=BN_{i,j}^{n} \tag{60}$$

$$BN_{i,j}^{n}=\left[\left(\left(2,0\upsilon_{t_{i,j}}^{n}\frac{v_{i,j+1}^{n}}{\Delta y}\right)-\frac{2}{3}SDS_{i,j}^{n}\right)-\left(-\left(2,0\upsilon_{t_{i,j-1}}^{n}\frac{v_{i,j-1}^{n}}{\Delta y}\right)-\frac{2}{3}SDS_{i,j-1}^{n}\right)\right]\frac{1}{\Delta y}$$
$$+\left[\frac{\left(\upsilon_{t_{i+1,j}}^{n}+\upsilon_{t_{i+1,j-1}}^{n}\right)}{2}\left(\frac{\left(u_{i+1,j}^{n}+u_{i,j+2}^{n}\right)}{2}-\frac{\left(u_{i+1,j-1}^{n}+u_{i+2,j-1}^{n}\right)}{2}\right)\frac{1}{\Delta y}\right.$$
$$\left.-\frac{\left(\upsilon_{t_{i-1,j}}^{n}+\upsilon_{t_{i-1,j-1}}^{n}\right)}{2}\frac{\left(u_{i-1,j}^{n}+u_{i,j}^{n}\right)}{2}-\frac{\left(u_{i-1,j-1}^{n}+u_{i,j-1}^{n}\right)}{2}\frac{1}{dy}\right]\frac{1}{2\Delta x} \tag{61}$$
$$+\frac{\left(\upsilon_{t_{i,j}}^{n}+\upsilon_{t_{i,j-1}}^{n}\right)}{2}\left(u_{i+1,j}^{n}+u_{i-1,j}^{n}\right)\frac{1}{\Delta x}\frac{1}{\Delta x}$$

Turbulent kinetic-energy transport (k) equation discretization

The turbulent kinetic-energy transport equations discretized on the staggered grid are written as follows:

$$\frac{Dk}{Dt}=\frac{\partial k}{\partial t}+u\frac{\partial k}{\partial x}+u\frac{\partial k}{\partial y}=\frac{\partial}{\partial x}\left(\frac{\upsilon_t}{\sigma_k}\frac{\partial k}{\partial x}\right)+\frac{\partial}{\partial y}\left(\frac{\upsilon_t}{\sigma_k}\frac{\partial k}{\partial y}\right)+P_{kh}+P_{kv}-\varepsilon$$
$$P_{kh}=\upsilon_t\left[2\left(\frac{\partial u}{\partial x}\right)^2+2\left(\frac{\partial v}{\partial y}\right)^2+2\left(\frac{\partial u}{\partial y}+\frac{\partial v}{\partial x}\right)^2\right]$$
$$P_{kv}=\left[\left(c_f+\frac{ac_dh}{2}\right)\left(u^2+v^2\right)\right]^{1.5}\Big/l \tag{62}$$
$$\frac{\partial k}{\partial t}=-\left(u\frac{\partial k}{\partial x}+u\frac{\partial k}{\partial y}\right)+\frac{\partial}{\partial x}\left(\frac{\upsilon_t}{\sigma_k}\frac{\partial k}{\partial x}\right)+\frac{\partial}{\partial y}\left(\frac{\upsilon_t}{\sigma_k}\frac{\partial k}{\partial y}\right)+P_{kh}+P_{kv}-\varepsilon$$

$$\frac{\partial k}{\partial t}=+SA0_{i,j}^{n}+SAN_{i,j}^{n}+SAPS_{i,j}^{n}+SAPD_{i,j}^{n}-SEP_{i,j}^{n} \tag{63}$$

Term on LHS

$$\frac{\partial k}{\partial t}=\frac{k_{i,j}^{n+1}-k_{i,j}^{n}}{\Delta t} \tag{64}$$

First term on RHS

$$-\left(u\frac{\partial k}{\partial x}+u\frac{\partial k}{\partial y}\right)=SA0_{i,j}^{n} \tag{65}$$

$$SA0_{i,j}^{n} = -\left[\begin{array}{l} \frac{\left(u_{i,j}^{n}+u_{i+1,j}^{n}\right)}{\Delta x}\frac{\left[-k_{i+2,j}^{n}+8\left(k_{i+1,j}^{n}-k_{i-1,j}^{n}\right)+k_{i-2,j}^{n}\right]}{12} \\ +\alpha\frac{ABS\left(u_{i,j}^{n}+u_{i+1,j}^{n}\right)}{\Delta x}\frac{\left[k_{i+2,j}^{n}-4\left(k_{i+1,j}^{n}+k_{i-1,j}^{n}\right)+6k_{i,j}^{n}+k_{i-2,j}^{n}\right]}{12} \\ +\frac{v_{i,j}^{n}+v_{i,j+1}^{n}}{\Delta y}\frac{\left[-k_{i,j+2}^{n}+8\left(k_{i,j+1}^{n}-k_{i,j-1}^{n}\right)+k_{i,j-2}^{n}\right]}{12} \\ +\alpha\frac{ABS\left(v_{i,j}^{n}+v_{i,j+1}^{n}\right)}{\Delta y}\frac{\left[k_{i,j+2}^{n}-4\left(k_{i,j+1}^{n}+k_{i,j-1}^{n}\right)+6k_{i,j}^{n}+k_{i,j-2}^{n}\right]}{12} \end{array}\right] \tag{66}$$

Second term on RHS

$$\frac{\partial}{\partial x}\left(\frac{\upsilon_t}{\sigma_k}\frac{\partial k}{\partial x}\right)+\frac{\partial}{\partial y}\left(\frac{\upsilon_t}{\sigma_k}\frac{\partial k}{\partial y}\right)=SAN_{i,j}^{n} \tag{67}$$

$$\begin{aligned} SAN_{i,j}^{n} &= \upsilon_{t_{i,j}}^{n}\frac{\left(k_{i+1,j}^{n}+k_{i-1,j}^{n}\right)}{\left(\Delta x\right)^{2}}+\left(\upsilon_{t_{i+1,j}}^{n}+\upsilon_{t_{i-1,j}}^{n}\right)\frac{\left(k_{i+1,j}^{n}+k_{i-1,j}^{n}\right)}{4\left(\Delta x\right)^{2}}+\upsilon_{t_{i,j}}^{n}\frac{\left(k_{i,j+1}^{n}+k_{i,j-1}^{n}\right)}{\left(\Delta y\right)^{2}} \\ &\quad+\left(\upsilon_{t_{i,j+1}}^{n}+\upsilon_{t_{i,j-1}}^{n}\right)\frac{\left(k_{i,j+1}^{n}+k_{i,j-1}^{n}\right)}{4\left(\Delta y\right)^{2}} \end{aligned} \tag{68}$$

Third term on RHS

$$P_{kh}=\upsilon_t\left[2\left(\frac{\partial u}{\partial x}\right)^{2}+2\left(\frac{\partial v}{\partial y}\right)^{2}+2\left(\frac{\partial u}{\partial y}+\frac{\partial v}{\partial x}\right)^{2}\right]=SAPS_{i,j}^{n} \tag{69}$$

$$\begin{aligned} SAPS_{i,j}^{n} &= \upsilon_{t_{i,j}}^{n}\left[2\left(\frac{\left(u_{i+1,j}^{n}+u_{i+2,j}^{n}-u_{i-1,j}^{n}+u_{i,j}^{n}\right)}{2\Delta x}\right)^{2}+2\left(\frac{\left(v_{i,j+1}^{n}+v_{i,j+2}^{n}-v_{i,j-1}^{n}+v_{i,j}^{n}\right)}{2\Delta y}\right)^{2}\right. \\ &\quad\left.+\left(\frac{\left(u_{i,j+1}^{n}+u_{i+1,j+1}^{n}-u_{i,j-1}^{n}+u_{i+1,j-1}^{n}\right)}{2\Delta y}+\frac{\left(v_{i+1,j}^{n}+v_{i+1,j+1}^{n}-v_{i-1,j}^{n}+u_{i-1,j+1}^{n}\right)}{2\Delta y}\right)^{2}\right. \end{aligned} \tag{70}$$

Fourth term on RHS

$$P_{kv}=\left[\left(c_f+\frac{ac_dh}{2}\right)\left(u^2+v^2\right)\right]^{3/2}\Big/\,l=SAPD_{i,j}^{n} \tag{71}$$

$$SAPD_{i,j}^{n}=\frac{\left[\left(gn^2\left(h_{i,j}^{n}\right)^{-1/3}+\frac{2.86*1.2}{2}\left(\eta_{i,j}^{n}+h_{i,j}^{n}\right)\right)\left(\left(u_{i,j}^{n}+u_{i+1,j}^{n}\right)^{2}+\left(v_{i,j}^{n}+v_{i,j+1}^{n}\right)^{2}\right)\right]^{3/2}}{\alpha h_{i,j}^{n}} \tag{72}$$

Fifth term on RHS

$$C_d\frac{k^{3/2}}{l}=SEP_{i,j}^{n} \tag{73}$$

$$SEP_{i,j}^{n}=C_d\frac{\left(k_{i,j}^{n}\right)^{3/2}}{\alpha h_{i,j}^{n}} \tag{74}$$

with stability criteria

$$\Delta t\leq\frac{1}{\frac{3}{2}\left(\frac{|u|}{\Delta x}+\frac{|v|}{\Delta y}\right)+\frac{2\upsilon_t}{(\Delta x)^2}+\frac{2\upsilon_t}{(\Delta y)^2}} \tag{75}$$

The Test Case, Results and Discussion

Numerical simulation was performed with the following input conditions matched to Dittrich & Schnauder laboratory experiments (2002 and 2004) (Table 1), as comparison and code verification are possible. White noise, the magnitude of which was 1% of the velocity of flow in the main channel, was imposed at the boundary to stimulate the development of horizontal vortices.

Temporal development of horizontal vortices

The development of horizontal vortices can be described using numerical computation as follows:

1. The longitudinal wavelength of vortices varies between 60 cm and 110 cm in statistical equilibrium (Figures 6 and 7).

2. The velocity and vorticity fields as shown in Figure 8 and 9, respectively, at several times (t = 10 s, t = 30 s, t = 60 s, t = 90 s, t = 120 s, and t = 150 s), indicating that small-scale horizontal vortices appeared first and then grew by merging with each other. In the beginning flow appears weak, with the corresponding accumulation of vortices in 5 regions. After t = 90 s, the spatial pattern of velocity and vorticity reached an equilibrium state in which 2 large vortices formed.

3. The values of the wavelength, both experimental and simulated, are shown in Table 2. The mean value of the wavelength of the predicted vortices (simulation) at the observation point was 61.4 cm. The corresponding length was 58.6, which agrees with the prediction. The calculation for finding the time period (T) of the wavelength was performed with fast Fourier transformation (FFT).

4. Figure 10 shows that the regions with water surface depression nearly coincided with the central parts of the horizontal vortices.

Table 1. Computational domain and grid size and time step.

Channel Width (B)	40 cm	Roughness (n)	0.0103	Transverse domain size	40 cm
Slope (I)	1.0×10^{-3}	Longitudinal domain size	15 m	Transverse grid size (Δy)	0.5 cm
Main channel depth (H_m)	6.0 cm	Longitudinal grid size (Δx)	1.0 m	Time step (Δt)	0.01

Table 2. Comparison value of wavelength (λ).

	u (cm/s)	Re	Froude	T (s)	λ measured (cm)
Simulation	23.9675	14381	0.312	2.56	61.4
Measured	20.55	12330	0.268	2.85	58.6

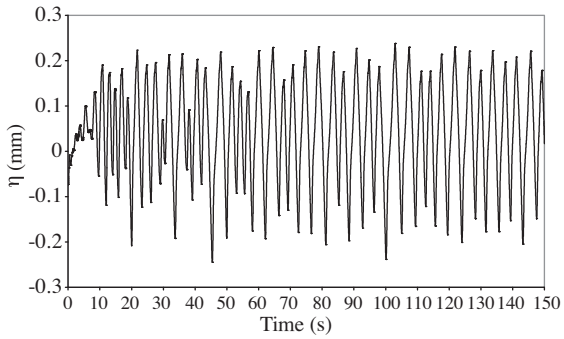

Figure 6. Variation in water surface elevation at the measurement point (numerical calculation).

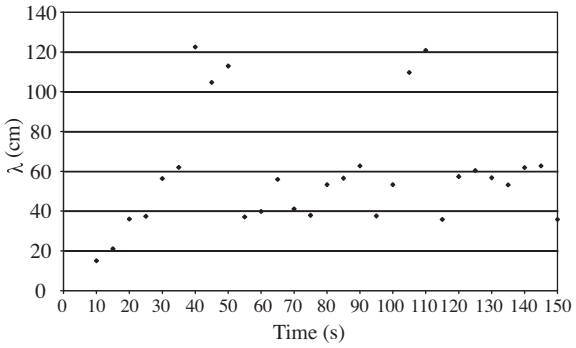

Figure 7. Variation in wave length at the measurement point (numerical calculation).

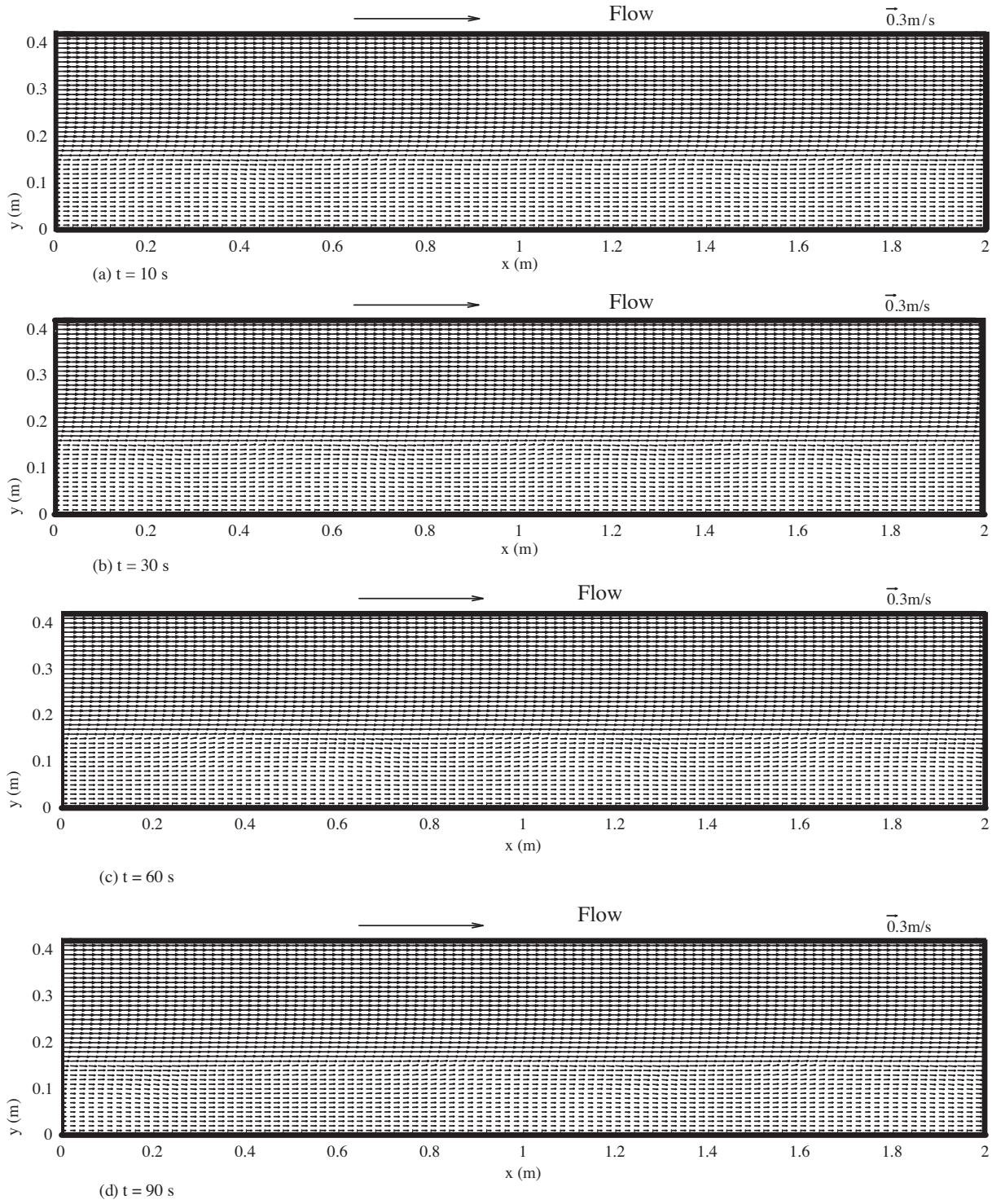

Figure 8. Temporal development of horizontal vortices. Spatial distribution velocity at (a) t = 10 s, (b) t = 30 s, (c) t = 60 s, (d) t = 90 s, (e) t = 120 s, (f) t = 150 s.

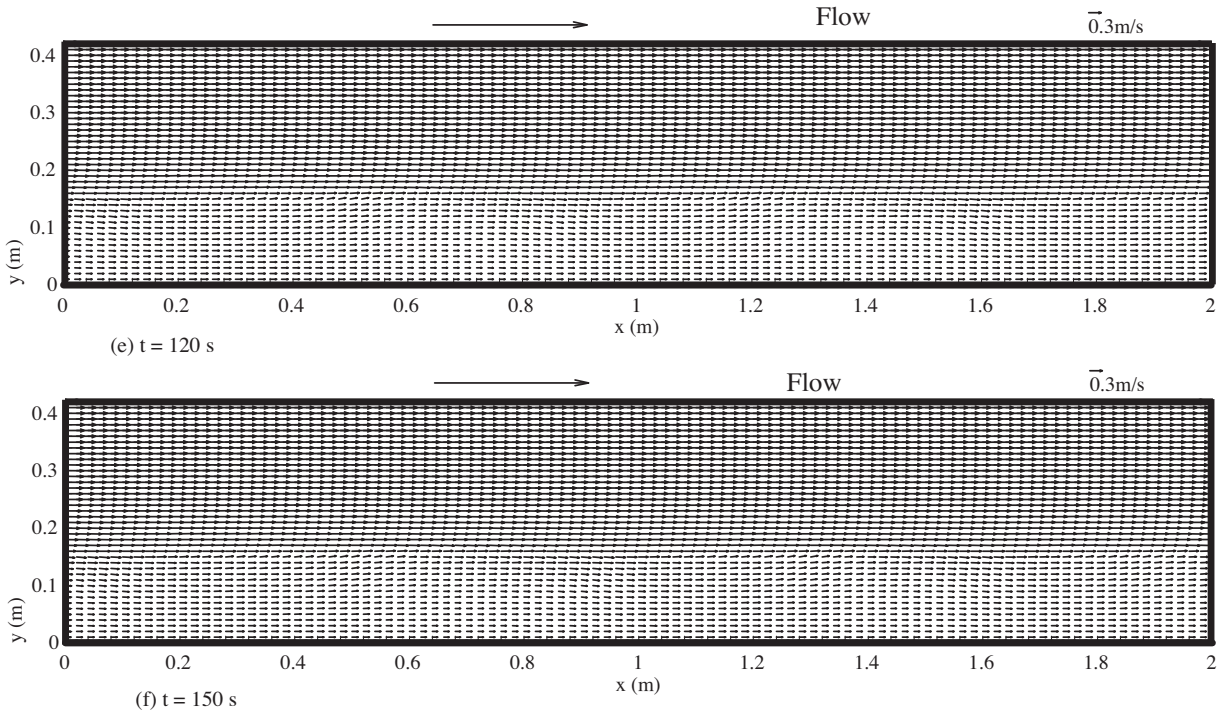

Figure 8. Continued.

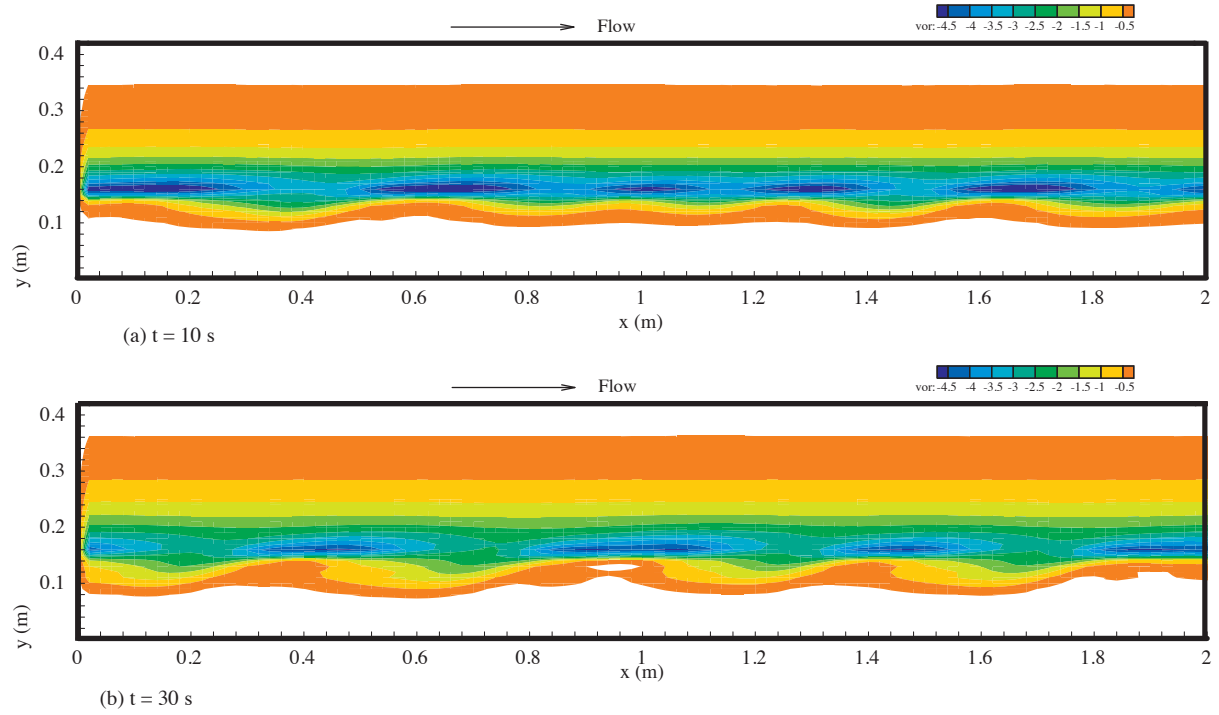

Figure 9. Temporal development of horizontal vortices. Spatial distribution vorticity at (a) t = 10 s, (b) t = 30 s, (c) t = 60 s, (d) t = 90 s, (e) t = 120 s, (f) t = 150 s.

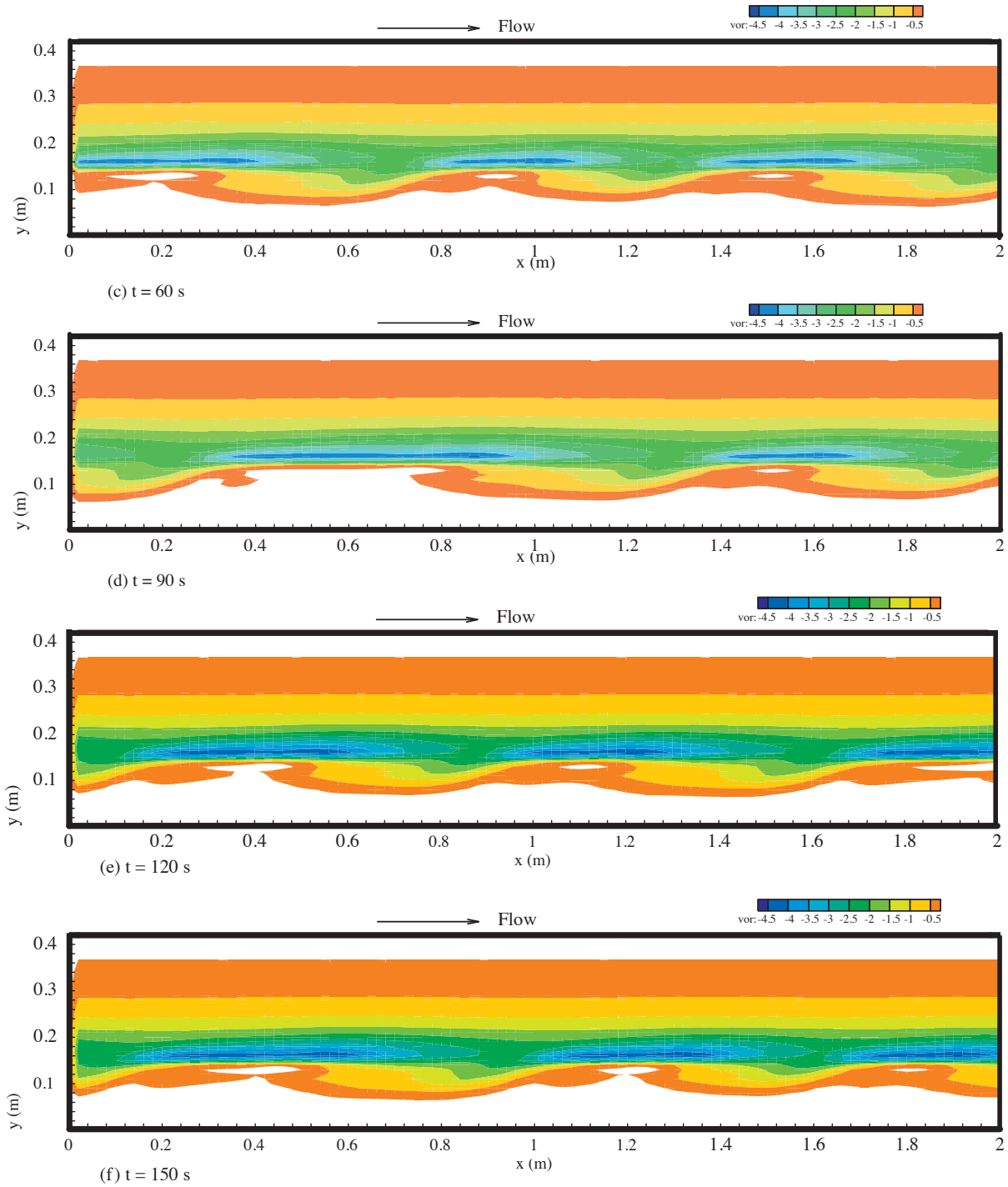

Figure 9. Continued.

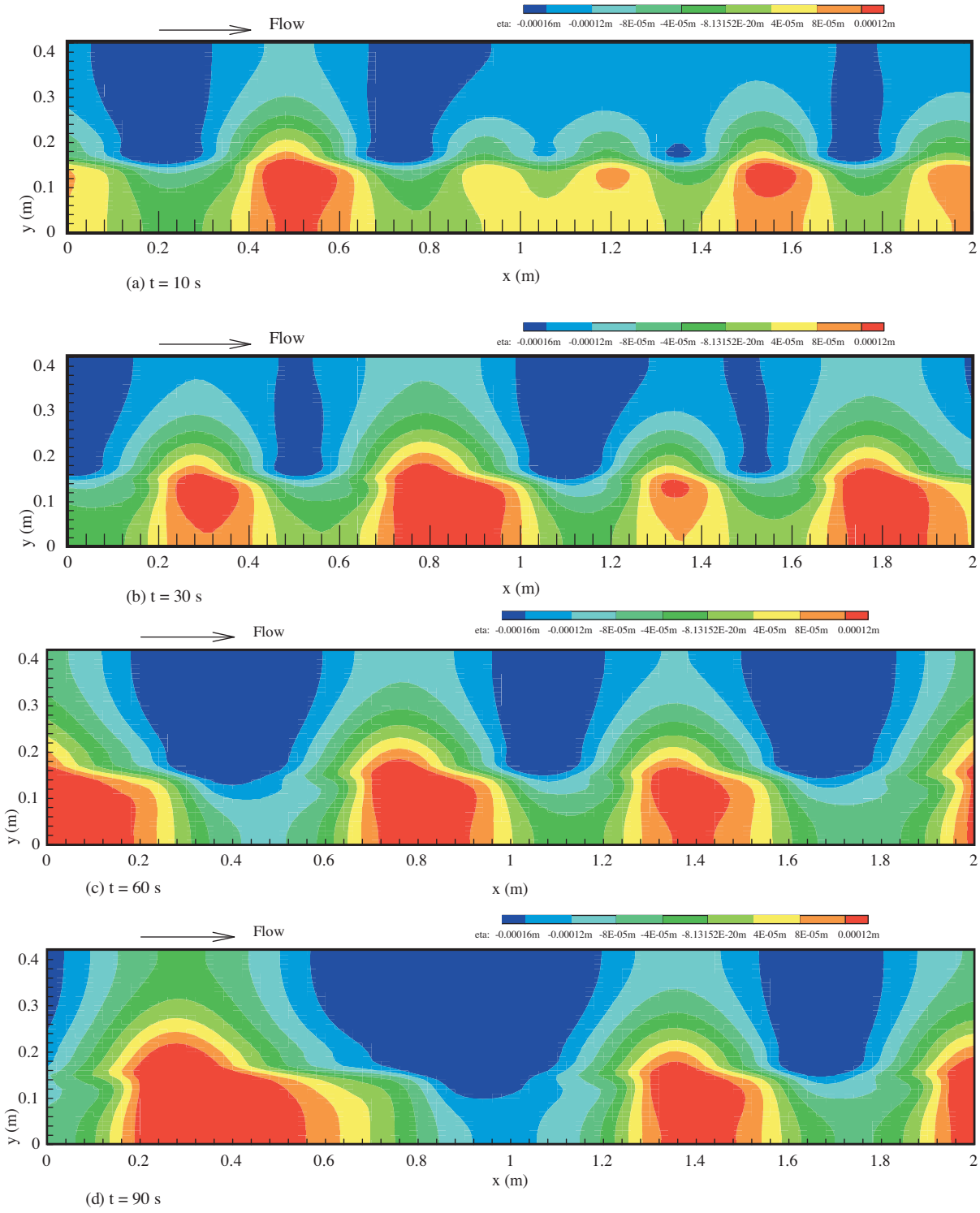

Figure 10. Temporal development of horizontal vortices. Spatial distribution of water surface η at (a) t = 10 s, (b) t = 30 s, (c) t = 60 s, (d) t = 90 s, (e) t = 120 s, (f) t = 150 s.

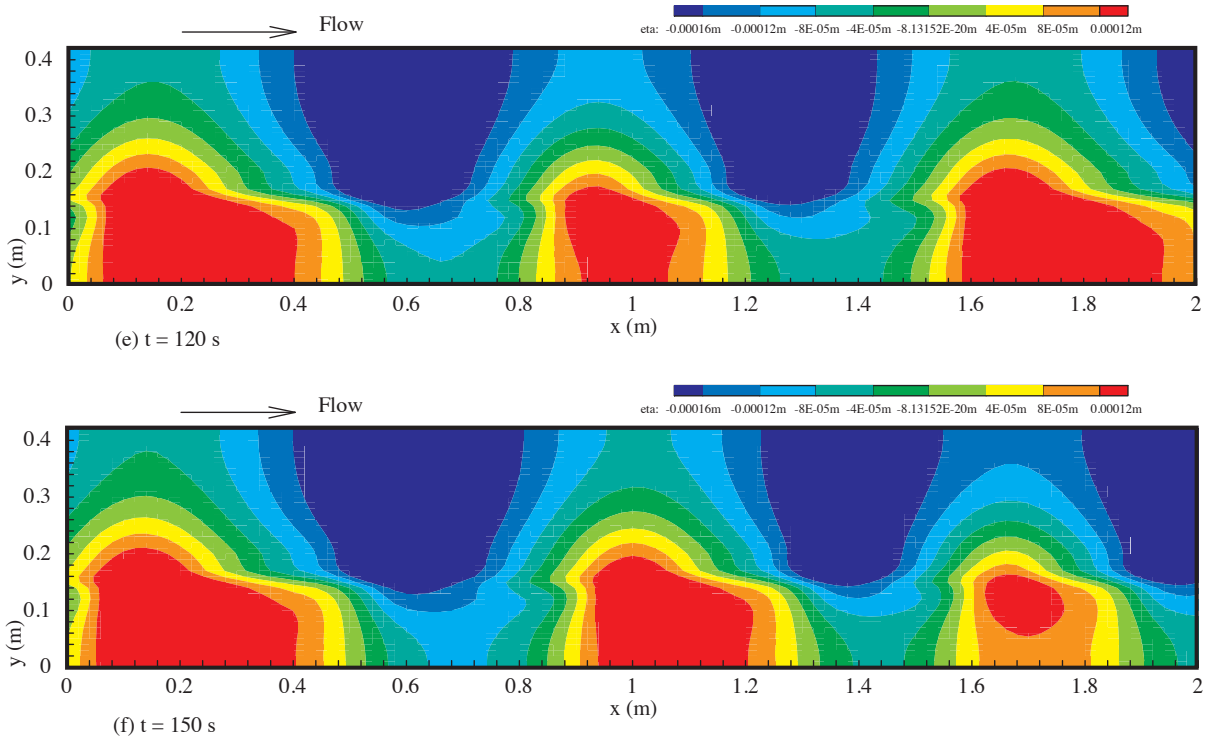

Figure 10. Continued.

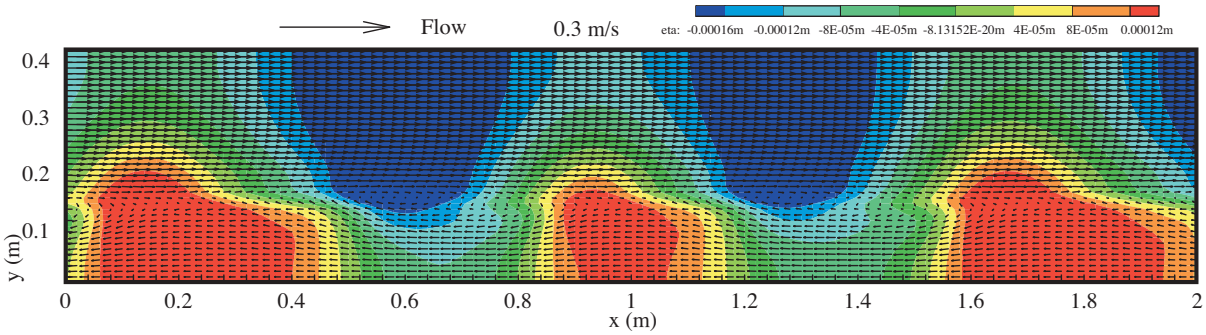

Figure 11. 2D velocity with water surface contour.

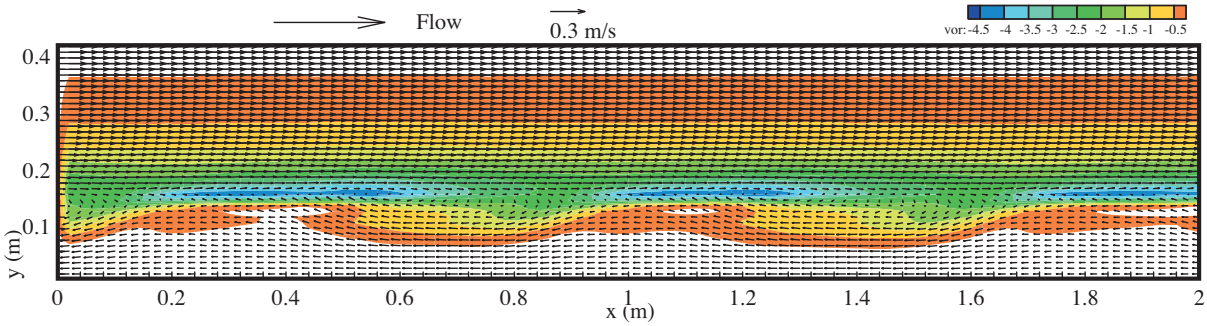

Figure 12. 2D velocity with vorticity contour.

Instantaneous flow field

The instantaneous 2D velocity with water surface contour and vorticity field is depicted in Figure 11 and 12, respectively, in which the velocity field is seen in the frame moving with the temporally averaged velocity at the boundary of the main channel and the flood channel (y = 16 cm). The maximum vorticity was located upstream of the geometrical center of the vortex. The vortices are inclined toward the longitudinal direction, which is important in producing the Reynolds stress.

Conclusion

The LES 2DH FLOWER_SD model was used to study lateral momentum transfer in a compound channel in which the instantaneous structure of horizontal vortices and temporally averaged velocity distribution had significant effects.

The results show that the horizontal vortices occurred at the boundary between the main channel and the flood channel, where significant mass and momentum exchange occurred.

The present model was proven to be a useful tool for engineering applications.

Acknowledgement

We gratefully acknowledge Dr. Ingo Schnauder and his colleagues at the Leibniz-Institute of Freshwater Ecology and Inland Fisheries, Germany for permission to use their laboratory experimental data, graphs, and technical notes.

Nomenclature

a	vegetation density parameter
B	channel width
Bf	flood channel width
Bm	main channel width
c_f	bottom friction coefficient
C_μ	a numerical constant
C_d	a numerical constant
g	gravitational acceleration
h	mean water depth
H	total water column height
Hf	flood channel depth
Hm	main channel depth
I	longitudinal channel bed slope
l	length scale of SDS turbulence
n	Manning's coeficient
p	pressure
p_a	pressure at the free surface t = time
α	a numerical constant
β	Boussinesq coefficient
δij	Kronecker
ε	dissipation rate of kinetic energy
η	water surface displacement
λ	wave length
μ	dynamic viscosity
ρ	water density
σ_k	a numerical constant
υ_t	eddy viscosity
τ_{bx}	bottom shear stress in (x dir.)
τ_{by}	bottom shear stress in (y dir.)
U	velocity in x direction
u	depth averaged velocity in x direction
V	velocity in x direction
v	depth averaged velocity in y direction
S_0	longitudinal channel bed slope (x direction)
w	depth averaged velocity in z direction
p_{kh}	energy production rate of turbulence due to horizontal shear
p_{kv}	energy production rate of turbulence due to vertical shear (bottom friction)
$\overline{u}$	mean (RANS) or large scale (LES) velocity in x direction
u'	fluctuation (RANS) or small scale/subgrid-scale (LES) velocity in x direction
$\overline{v}$	mean (RANS) or large scale (LES) velocity in y direction
v'	fluctuation (RANS) or small scale/subgrid-scale (LES) velocity in y direction
$\overline{w}$	mean (RANS) or large scale (LES) velocity in z direction
w'	fluctuation (RANS) or small scale/subgrid-scale (LES) velocity in z direction

References

Bousmar, D., "Flow Modelling in Compound Channels, Momentum Transfer Between Main Channel and Prismatic or Non-Prismatic Floodplains" , *Thesis for Doctor's Degree*, Faculté des Sciences Appliquées, Unité de Génie Civil et Environemental, Université catholique de Louvain, France, 2002.

Deardorf, J.W., "A Numerical Study of Three-Dimensional Turbulent Channel Flow at Large Reynolds Numbers." Journal Fluid Mech., Cambridge, England, UK, 41, 453-480, 1970.

Dittrich, A. and Schnauder, I., "Physical Modelling of Compound Channel Flow with Rigid and Flexible Cylindrical Floodplain Vegetation", European Geophysical Society, Annual Meeting, Nice, France, Abstract #4541, 2002.

Dittrich, A. and Schnauder, I., "Interaction Processes in a Straight Compound Channel With Rigid and Flexible Emergent Floodplain Vegetation", Riverflow 2004, Naples, Italy, Proceedings Volume 1, 347-352, 2004.

Ikeda, S., Ohta K. and Hasegawa, H., "Instability-Induced Horizontal Vortices in Shallow Open-Channel Flows with an Inflection Point in Skewed Velocity Profile." J. Hydroscience and Hydraulic Engineering Tech., Japan Society of Civil Engineers, 12, 69-84, 1994.

Ikeda, S., "Invited Lecture: Role of Lateral Eddies in Sediment Transport and Channel Formation." River Sedimentation, Jayawardena, Lee & Wang, eds., Balkema, Rotterdam, 195-205, 1999.

Leonard, A. "On the Energy Cascade in Large-Eddy Simulations of Turbulent Fluid Flows." Technical Report Rep. TF-1, Thermosciences Div., Stanford University, Dept. Mech. Eng., Stanford, CA 94305, California, 1973.

Liggett, J.A. Fluid Mechanics. McGraw Hill, New York, 1994.

McDonough, J. M., "Introductory Lectures on Turbulence, Physics, Mathematics and Modeling." Lecturer Notes, Departments of Mechanical Engineering and Mathematics, University of Kentucky, Kentucky, 2004.

McDonough, J.M., "Lectures on Computational Numerical Analysis of Partial Differential Equations." Lecturer Notes, Departments of Mechanical Engineering and Mathematics, University of Kentucky, United State of America, 1985.

McKibben, J.F., "A Computational Fluid Dynamics Model for Transient Three-Dimensional Free Surface Flows." Thesis for Doctoral Degree, Institute of Paper Science and Technology, Atlanta, Georgia, 1993.

Nadaoka, K. and Yagi, H., "Shallow Water Turbulence Modeling and Horizontal Large-Eddy Computation of River Flow." Journal of Hydraulic Engineering, ASCE, 124, 493-500, 1998.

Rastogi, A.K. and Rodi, W. "Predicitons of Heat and Mass Transfer in Open Channels." Journal of the Hydraulics Division, ASCE, 104, 397-420, 1978.

Rodi, W. Turbulence Models and Their Application In Hydraulics: A State of the Art Review. IAHR Book Publications, Delft. 1980.

Riddaway, R.W, "Numerical Methods", Meteorological Training Course Lecture Series, ECMWF, 2001.

Salvetti, M.V. and Banerjee, S. "A Priori Tests of a New Dynamic Subgrid-Scale Model for Finite-Difference Large Eddy Simulations", Phys. Fluids, 7 (11), 1995.